Measuring Rectilinearity

Paul L. Rosin
Cardiff School of Computer Science
Cardiff University
Cardiff
U.K.
Paul.Rosin@cs.cf.ac.uk

Joviša Žunić*
Computer Science Department
Exeter University
Harrison Building
Exeter EX4 4QF
U.K.
J.Zunic@exeter.ac.uk

Abstract

Two new methods for computing the rectilinearity of polygons are presented. They provide shape measures and estimates of canonical orientations which can be used in applications such as shape retrieval, object classification, image segmentation, etc. Examples are presented demonstrating their use in skew correction of scanned documents, deprojection of aerial photographs of buildings, and scale selection for curve simplification. Furthermore, testing has been carried out on synthetic data and with human subjects to verify that the measures do indeed produce perceptually meaningful results.

Index Terms– shape descriptor, polygon, rectilinear

1 Introduction

Shape is used in many instances of data processing. Take for example medical imaging of the brain: shape is used for segmentation of the cortical surface prior to functional brain mapping [11]; the shape of the cerebral cortex (its degree of folding) can distinguish normal and abnormal fetal brains [1]; and the shape of the corpus callosum was used to analyse deficits due to fetal alcohol exposure [4]. There are a myriad of other applications: characterising large and small submarine volcanoes [17], measuring cherry fruit shape [2], analysing the molecular structure of gold [24], and optimising aerodynamic design [7] to name but a few.

In computer vision shape has been a long standing topic of research [19, 14], and many schemes have been developed. However, for the particular aspect of shape covered in this paper, namely measures for *rectilinearity*[1], there has been little previous research. Nevertheless, rectilinear shapes obviously occur frequently in manufactured environments, and moreover the human visual system is particularly tuned to right angles [8]. In a recent paper Žunić and Rosin [25] gave two possible definitions of measures of rectilinearity of an arbitrary polygon P:

$$\mathcal{R}_1(P) = \frac{4}{4-\pi} \cdot \left(\max_{\theta \in [0,2\pi]} \frac{\mathcal{P}er_2(P)}{\mathcal{P}er_1(P,\theta)} - \frac{\pi}{4} \right)$$

$$\mathcal{R}_2(P) = \frac{\pi}{\pi - 2\cdot\sqrt{2}} \cdot \left(\max_{\theta \in [0,2\pi]} \frac{\mathcal{P}er_1(P,\theta)}{\sqrt{2}\cdot\mathcal{P}er_2(P)} - \frac{2\cdot\sqrt{2}}{\pi} \right),$$

where $\mathcal{P}er_2(P)$ denotes the Euclidean perimeter of P, and $\mathcal{P}er_1(P)$ denotes the perimeter of P in the sense of the L_1 norm. $\mathcal{P}er_1(P,\theta)$ is the L_1 perimeter of the polygon obtained by rotating P by the angle θ with the origin as the centre

*Joviša Žunić is also with the Mathematical Institute of the Serbian Academy of Sciences and Arts, Belgrade

[1]Many dictionary definitions of rectilinearity are vague, e.g. "Composed by straight lines". In this paper the more precise sense of a rectilinear polygon such that it is composed of horizontal or vertical segments is used.

of rotation. The measures are such that they lie in the range $(0, 1]$, return the peak value of one only for rectilinear polygons, and moreover they are invariant under similarity transformations of P.

Žunić and Rosin [25] demonstrated the integration of the rectilinearity measures into snakes to perform boundary refinement, increasing the rectilinearity of noisy regions extracted from images. They also used it as part of a feature vector in a trademark matching example. Further applications of rectilinearity measures are possible, the most obvious being classification. Also in certain situations it can be used as an alternative to convexity in segmentation [18], shape partitioning [23], grouping [13], etc.

Hand in hand with computing rectilinearity values, the rectilinearity measures provide a means of determining canonical orientations for shapes. In many applications such an orientation is useful as a first step in the analysis of shapes, and this is often provided by the moments based principal axis. In contrast, the orientation maximising rectilinearity is based more on local shape properties while the principal axis only reflects the gross spatial distribution. The difference between the two is demonstrated in figure 1 where the the rectilinearity based orientation appears more appropriate than that computed using moments. Further related examples will be shown in the experimental results section.

(a) (b)

Figure 1: A shape placed in its canonical orientation using (a) $\mathcal{R}_1$, (b) moments.

2 New Rectilinearity Measures

Žunić and Rosin [25] demonstrated that their rectilinearity measures performed well [25], but there were no alternative measures available for comparison against. In contrast, for measures such as circularity/compactness many formulations exist [3, 5, 10, 20, 6]. Therefore, in this paper we describe two new rectilinearity measures based on different properties of the polygon, namely angles rather than perimeter lengths as used in Žunić and Rosin's [25] previous rectilinearity measures.

2.1 An Angle Error Rectilinearity Measure

A simpler approach than reference [25] to measure rectilinearity would be to use the sum of the absolute differences in angles between edges modulo $\frac{\pi}{2}$ as an error term. Its limitation is that any polygons with the same angles have the same estimated rectilinearity which is not always acceptable (see figure 2). A possible correction would be to weight the angle

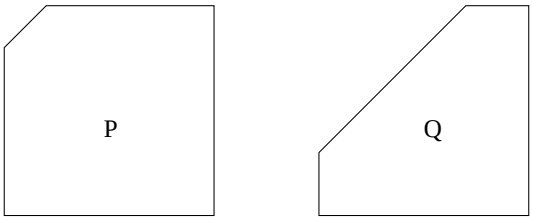

Figure 2: Two given 5-gons have identical angles, but P should have a higher estimated rectilinearity than Q.

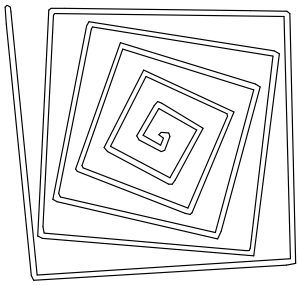

Figure 3: A spiral polygon which should not be considered rectilinear even though all its angles are close to $\frac{\pi}{2}$.

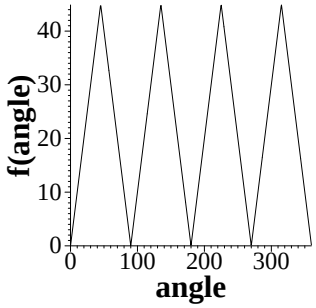

Figure 4: Function to compute discrepancy from multiples of $\frac{\pi}{2}$ (angles shown in degrees).

errors by their edge lengths. However, this remains unsatisfactory as shown by a polygon made up of a series of edges with increasing lengths, each making an angle slightly greater than $\frac{\pi}{2}$ with their neighbours (see figure 3). Although local errors are small the shape approximates a spiral, and in the limit as the number of edges increases all edge orientations will be included. Thus, despite having a low angular error it should actually receive a poor rectilinearity score. These difficulties suggest that one solution would be to calculate angles with respect to some global coordinate frame and measure discrepancies from multiples of $\frac{\pi}{2}$. Thus, if for a line of length l_i and orientation ϕ_i, the angular difference with respect to the coordinate frame's orientation of θ is $\alpha_i = \phi_i - \theta$. The discrepancy from multiples of $\frac{\pi}{2}$ is measured using the function $f(\alpha_i) = \min_n \left(|\alpha_i - n\frac{\pi}{2}|\right)$, where $n = 0, 1, \ldots, 4$ if $0 \leq \alpha_i \leq 2\pi$ (see figure 4). The measure is then computed as

$$\mathcal{R}_A = 1 - \min_\theta \frac{8}{\pi \sum l_i} \sum f(\phi_i - \theta) \cdot l_i$$

normalised so that values lie in the range $(0, 1]$. The normalisation factor of $\frac{8}{\pi}$ occurs since the largest possible summed angle discrepancy is obtained for the limiting case of a regular polygon as the number of sides increases and it approaches a circle. In that case the angle discrepancies will be uniformly distributed in the range $[0, \frac{\pi}{4})$, and so the mean value is $\frac{\pi}{8}$.

2.2 An Angle Variance Rectilinearity Measure

A second new rectilinearity shape measure that avoids the above problems is also described here. It operates on the assumption that the distribution of the shape's tangent orientations (in the range $[0, \pi]$) should contain two main peaks separated by $\frac{\pi}{2}$ radians. However, one peak may be much smaller than the other, e.g. for an elongated rectangle. Rather than search for two uneven peaks, the orientation histogram is superimposed on itself after a shift of $\frac{\pi}{2}$, creating a repeated cycle in the histogram. That is, the histogram is constructed by the following update for each line (length l_i and orientation ϕ_i): $H\left[\phi_i\right] = H\left[\phi_i\right] + l_i$ and $H\left[\phi_i + \frac{\pi}{2}\right] = H\left[\phi_i + \frac{\pi}{2}\right] + l_i$, taking into account that directional values wrap such that $\phi + \pi n \rightarrow \phi,\ n \in \mathcal{Z}$. Thus two correctly separated peaks will reinforce each other. Now only

a histogram section of width $\frac{\pi}{2}$ needs to be examined. For a highly rectilinear shape there should only be one narrow peak in the section. If the section is positioned so as to place the peak in its centre then the standard deviation will be low. Otherwise if the peak is off-centre it will wrap around the opposite ends of the section producing a high standard deviation. Thus, the canonical orientation is found by positioning the section to minimise the standard deviation and returning the mean orientation within that section.

$$\begin{aligned} \phi_{min} &= \arg \min_{\phi \in \left[0, \frac{\pi}{2}\right]} S_0 \left\{ H'\left[\phi\right] \ldots H'\left[\phi + \frac{\pi}{2}\right] \right\} \\ \phi_{canonical} &= \mu \left\{ H'\left[\phi_{min} - \frac{\pi}{4}\right] \ldots H'\left[\phi_{min} + \frac{\pi}{4}\right] \right\} \end{aligned}$$

Since directional data is being analysed the *circular* mean and standard deviation are used, where the circular variance is calculated as [15]

$$S_0 = 1 - \sqrt{C^2 + S^2}$$

and

$$C = \frac{1}{n} \sum_{i=1}^{n} \cos \phi, \quad S = \frac{1}{n} \sum_{i=1}^{n} \sin \phi$$

for a set of n orientation samples ϕ in the range $[0, 2\pi]$ (requiring the angles used above to be rescaled as 2ϕ to wrap around at π instead). The circular mean is calculated as

$$\mu = \begin{cases} \tan^{-1} \frac{S}{C} & \text{if } C \geq 0 \\ \pi + \tan^{-1} \frac{S}{C} & \text{if } C < 0 \end{cases} .$$

If i) there is a wide spread in the orientations, ii) the two dominant orientations are not separated by $\frac{\pi}{2}$, or iii) secondary orientation peaks are present, then the circular variance will be high. This suggests that the circular variance of the orientation histogram as described above can be used as a rectilinearity measurement.

In fact, since the two cycles in the histogram mean that the histogram windows do not need to wrap around the end, circular statistics are not necessary. However, we still use them since the values of S_0 are conveniently bounded in the range $[0, 1]$. To produce a response of unity for a rectilinear polygon and zero for a circle we use $\mathcal{R}_S = 1 - S_0$.

3 Considerations for Digital Data

(a) (b)

Figure 5: Two shapes (in gray) with local modifications (in black) causing a reversal in measured rectilinearity. a) The circle is quantised on a square grid. b) The rectangle has a series of semi-circles superimposed.

When working with real data quantisation effects need to be taken into consideration. For instance, if boundary curves are extracted from the image using 4-way connectivity then the resulting polygons are perfectly rectilinear. Nevertheless, despite matching the rectilinearity measure's criteria at the fine scale, at a coarser scale they may not be perceptually rectilinear. In fact, it is easy to construct various counter-examples (figure 5) that display a mismatch between global and local structure showing that the problem goes beyond quantisation errors. At the quantisation level a solution would be to characterise straight line segments so as to be able to identify sequences of chain codes as straight lines [12]. This still does not take noise and other distortions into account. Previously, curves extracted from images were pre-processed by generating a polygonal approximation to eliminate minor fluctuations [25]. This effectively eliminates the problem of digitisation artifacts of the type shown in figure 5a. More precisely, in all experiments Ramer's algorithm [21] with a threshold of three pixels was run.[2] This involved recursively subdividing the curve at the point of maximum deviation between the straight line segment between the ends of the curve segment until the maximum deviation was less than three.

An alternative method of coping with the effects of quantisation, noise, etc. is to blur the curve. It is known that if a curve is smoothed using the geometric heat flow equation it becomes more and more circular, eventually shrinking to a circular point in finite time [9]. Since the circle gives the lowest rectilinearity value this suggests that any increase in the measured rectilinearity of the blurred curve is not an artifact of the blurring, but actually reflects the true shape of the curve that has been "uncovered" by filtering out the distracting detail. It is not necessary to know the parameters describing the curve irregularities. Instead, the curve is smoothed by increasing amounts until it is convex, and the maximum rectilinearity value over this evolution is returned.

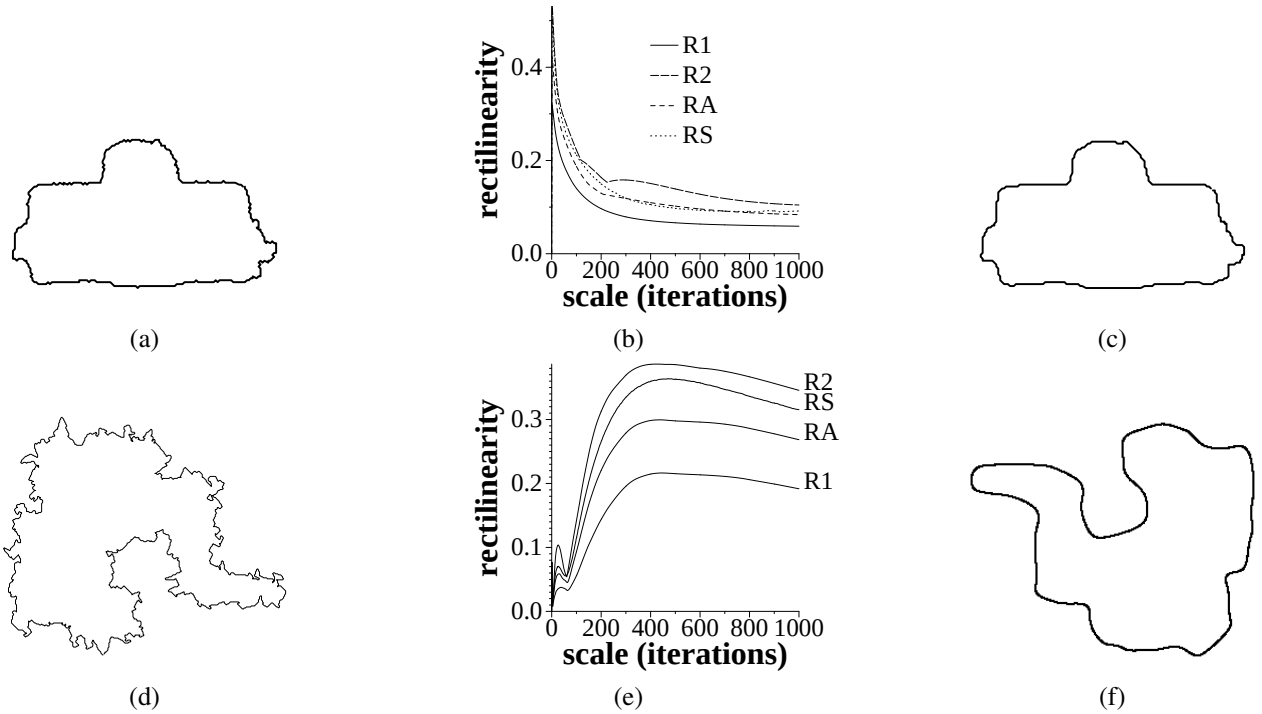

Figure 6: Eliminating noise by smoothing so as to maximise rectilinearity. a & d) original curve, b & e) rectilinearity versus scale, c & f) curves smoothed at optimal scale.

The effect on the rectilinearity measures of smoothing to overcome local structure problems of the type shown in figure 5a is demonstrated in figure 6, where a simple iterative Gaussian blurring procedure is used (at each iteration every coordinate is averaged with its immediate neighbours). In some cases (e.g. figure 6a–c) smoothing hardly improves the

[2] For removing just digitisation effects a lower polygonalisation threshold would be sufficient. However, a higher threshold value has been set since the polygonalisation stage is also being used to remove noise.

rectilinearity; all measures peaked at 2 smoothing iterations. At other times (e.g. figure 6d–f) smoothing removes the fine detail that would otherwise severely bias the rectilinearity value, and also correctly recovers the underlying rectilinear shape. As figure 6b & e show, all the rectilinearity measures respond in a similar manner to the smoothing, and the positions of the peaks varied in the range $[425, 472]$ iterations.

4 Some Examples

To test the effectiveness of the rectilinearity measures they are first applied to a (perfect) rectilinear polygon located as the left hand shape in figures 7–10 which is then degraded by adding increasing levels of local noise to the polygon's vertices. The examples show that the rectilinearity measure is well behaved; increasing distortion consistently decreases the computed value, with one minor exception in figure 10. Note also that the orientations maximising the inner terms of the rectilinearity measures (i.e. $\mathcal{Q}_1 = \frac{\mathcal{P}er_2(P)}{\mathcal{P}er_1(P,\theta)}$, $\mathcal{Q}_A = 1 - \frac{8}{\pi \sum l_i} \sum e_i(\theta) \cdot l_i$) match our expectations except at high noise levels when the rectilinearity measure has dropped close to zero. The scale based results in figure 8 demonstrate its better ability to cope with local noise.

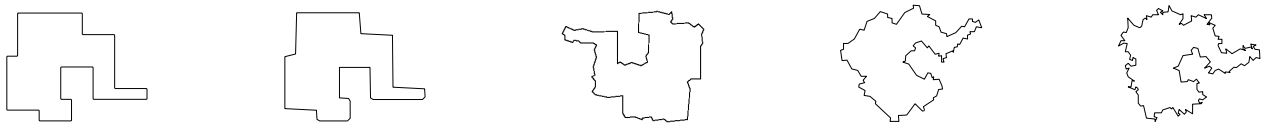

1.000 0.849 0.334 0.041 0.038

Figure 7: Examples of polygons with their rectilinearity measured using $\mathcal{R}_1$. Polygons are rotated to the orientations that maximised $\mathcal{Q}_1$.

1.000 0.853 0.477 0.382 0.216

Figure 8: Examples of polygons with their rectilinearity measured using $\mathcal{R}_1$ over scale. Polygons are rotated to the orientations that maximised $\mathcal{Q}_1$ over scale. The original curves are overlaid on the blurred version (drawn in gray) that optimised $\mathcal{R}_1$.

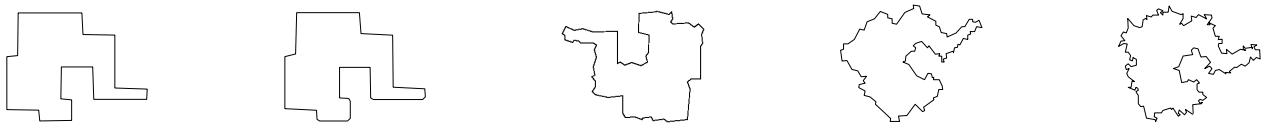

1.000 0.892 0.418 0.052 0.051

Figure 9: Examples of polygons with their rectilinearity measured using $\mathcal{R}_A$. Polygons are rotated to the orientation that maximised $\mathcal{Q}_A$.

The measures are now applied to a wide range of shapes, which are then ranked in order of decreasing rectilinearity (figures 11–14). Although many individual differences are evident, overall there are substantial similarities, and in general the mean difference in rank is only about two or three. It can be seen in figure 12 that the blurring process has not introduced counter-intuitive effects. Overall, the rankings look reasonable. Their correctness was tested more quantitatively by asking 22 human subjects to rank the 37 shapes according to rectilinearity [25].[3]

[3]The subjects were naive adults. The concept of rectilinearity was explained to them in two ways: a perfect rectilinear shape could be composed of

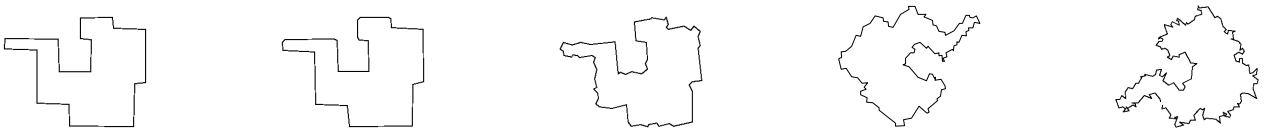

1.000 0.931 0.475 0.055 0.058

Figure 10: Examples of polygons with their rectilinearity measured using $\mathcal{R}_S$. Polygons are rotated by $\phi_{canonical}$.

Table 1 gives the correlations between the rectilinearity measures and the mean human ranking. Since the average correlation of individual humans relative to the mean human rankings was 0.799 then the rectilinearity measures can all be considered to perform as well as human judgements.

	$\mathcal{R}_1$	$\mathcal{R}_2$	$\mathcal{R}_S$	$\mathcal{R}_A$	$\mathcal{R}_1$ scale	$\mathcal{R}_2$ scale	$\mathcal{R}_S$ scale	$\mathcal{R}_A$ scale	human
$\mathcal{R}_1$	1.000	0.931	0.965	0.980	0.882	0.860	0.874	0.881	0.888
$\mathcal{R}_2$	–	1.000	0.985	0.978	0.884	0.896	0.900	0.901	0.831
$\mathcal{R}_S$	–	–	1.000	0.992	0.901	0.900	0.907	0.912	0.855
$\mathcal{R}_A$	–	–	–	1.000	0.899	0.889	0.900	0.904	0.859
$\mathcal{R}_1$ scale	–	–	–	–	1.000	0.975	0.973	0.993	0.881
$\mathcal{R}_2$ scale	–	–	–	–	–	1.000	0.987	0.990	0.882
$\mathcal{R}_S$ scale	–	–	–	–	–	–	1.000	0.983	0.863
$\mathcal{R}_A$ scale	–	–	–	–	–	–	–	1.000	0.884

Table 1: Rectilinearity algorithms and human performance compared using the Spearman rank-order correlation coefficient.

Several examples are now presented that demonstrate the ability of the rectilinearity measures to determine a canonical orientation. Figures 15a and 16a show scanned documents needing skew correction. After thresholding and elimination of the graphics and small regions (whose area is less than 20 pixels) the remaining region boundaries are shown in figures 15b and 16b. Note that due to the lower resolution of the latter image words are extracted as blocks whereas individual characters are retained in figure 15b. Polygons were analysed separately to determine their rectilinearity and canonical orientation. The orientations were weighted by the product of polygon rectilinearity and area, and the weighted circular (modulo $\frac{\pi}{2}$) mean orientation calculated. As seen in figures 15c and 16c this provides a good estimate for skew correction. All the measures ($\mathcal{R}_1$, $\mathcal{R}_2$, $\mathcal{R}_A$, $\mathcal{R}_S$), analysed over scale, produced very similar values: the standard deviation of orientation estimates amongst the four, averaged over a set of ten images, was 0.16°. If instead the polygons were simplified by Ramer's algorithm then the threshold needed to be kept small (e.g. less than 3) given the small size of the regions. Results were still good, but were more variable ($\sigma = 0.50^\circ$).

Although a rectilinearity based approach is less efficient than standard skew correction methods it would be able to cope better with certain types of pages, e.g. irregular line layout, equations, etc. Another example of more variable structure is given in the Digital Elevation Model (DEM) in figure 17. While the buildings are roughly rectilinear and laid out in part on a rectangular grid there are many variations. Again applying the rectilinearity measures, analysed over scale, produced consistent results, which enabled the image to be rotated to correctly align the majority of the buildings with the XY axes.

Extending the simple rotation of images the next example shows the deskewing of the outlines of the buildings extracted from the aerial photograph in figure 18a&b. Assuming orthographic projection the simple affine mapping $(x', y') = (x + \beta y, y)$ is used, and applied at orientations $\theta \in \left[0, \frac{\pi}{4}\right]$. Rectilinearity is maximised over β and θ, and

horizontal and vertical lines if oriented appropriately; alternatively, the internal angles should be $\pm 90^\circ$. No time limit was given, and the task typically took about five minutes. The shapes were presented as circular cut outs, randomly laid out so that there was no initial preferred orientation or ordering. It should be noted that while the first explanation defines rectilinearity according to a more global property, and the second implies a local measure, both were presented as equally valid descriptions.

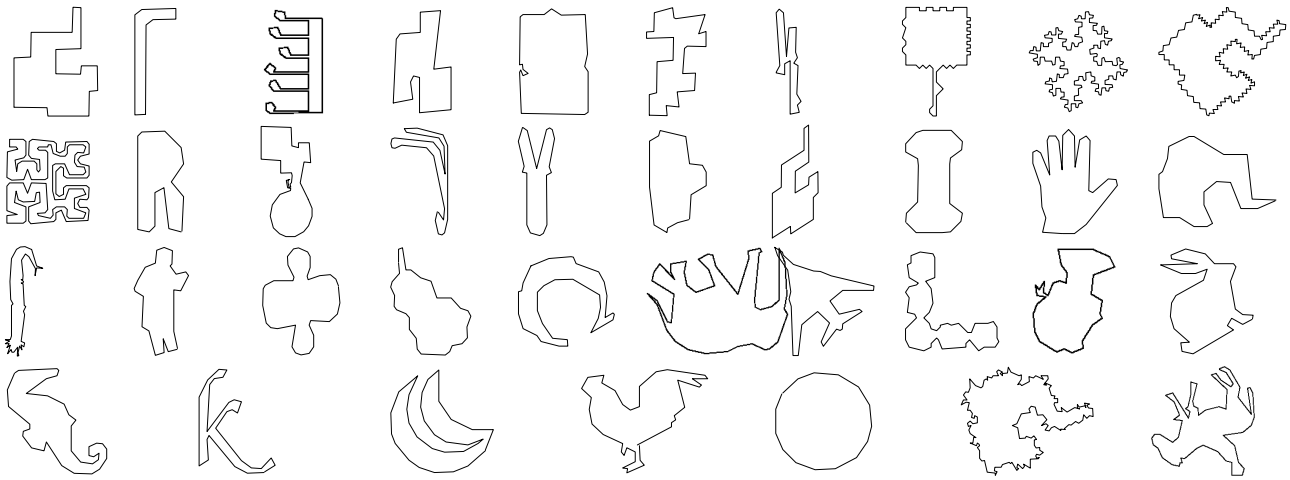

Figure 11: Shapes ranked by $\mathcal{R}_1$.

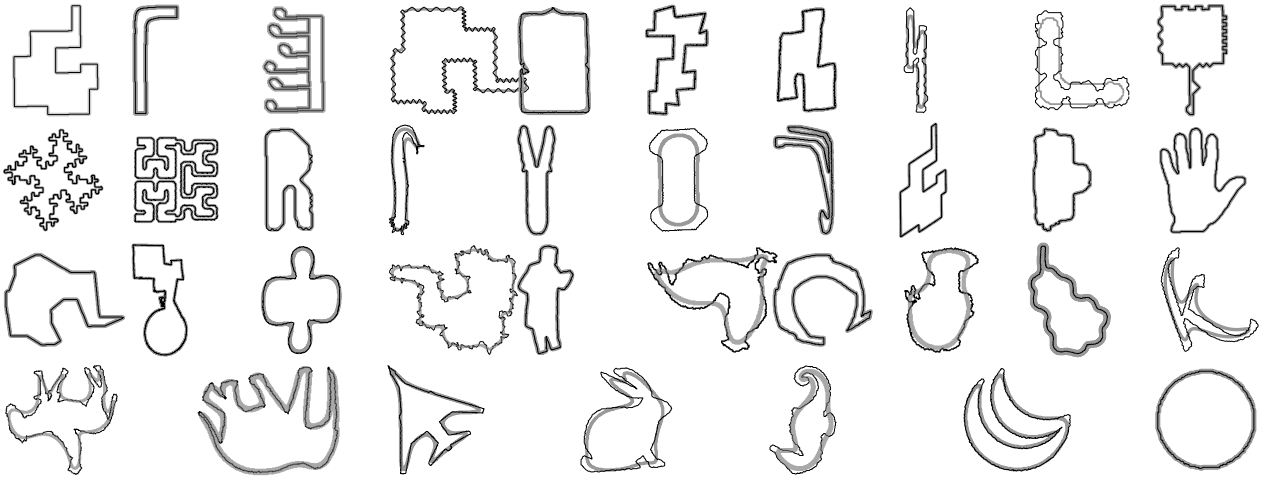

Figure 12: Shapes ranked by $\mathcal{R}_1$ maximised over scale. The curves are overlaid on the blurred version (drawn in gray) that optimised $\mathcal{R}_1$.

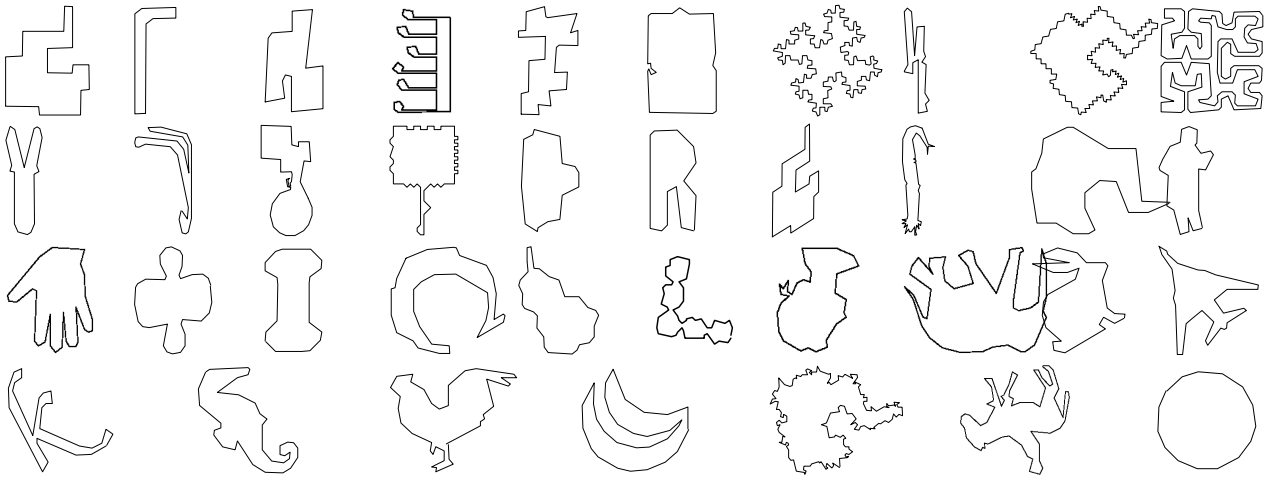

Figure 13: Shapes ranked by $\mathcal{R}_A$.

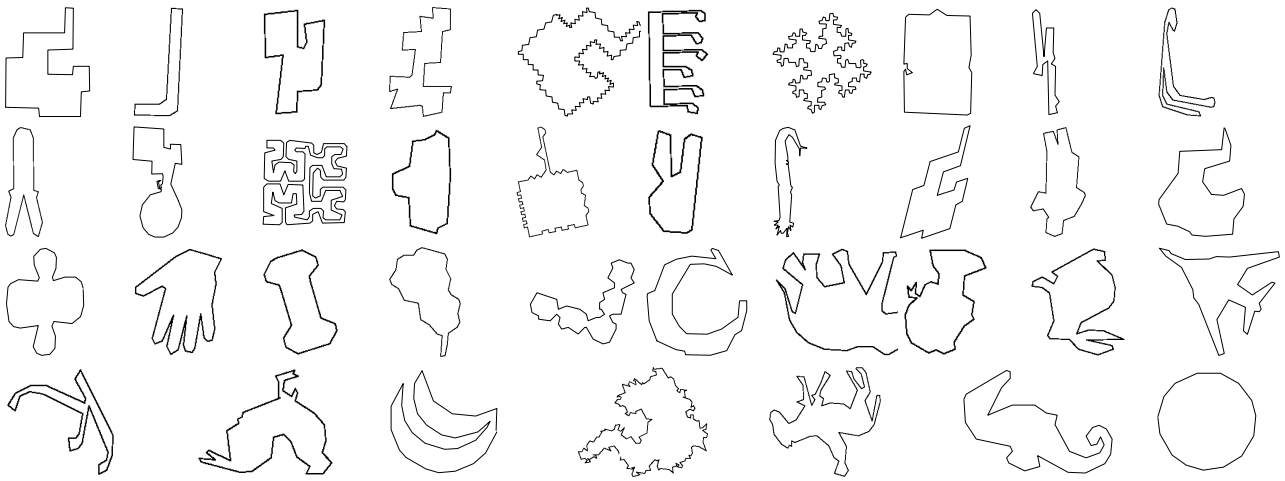

Figure 14: Shapes ranked by $\mathcal{R}_S$.

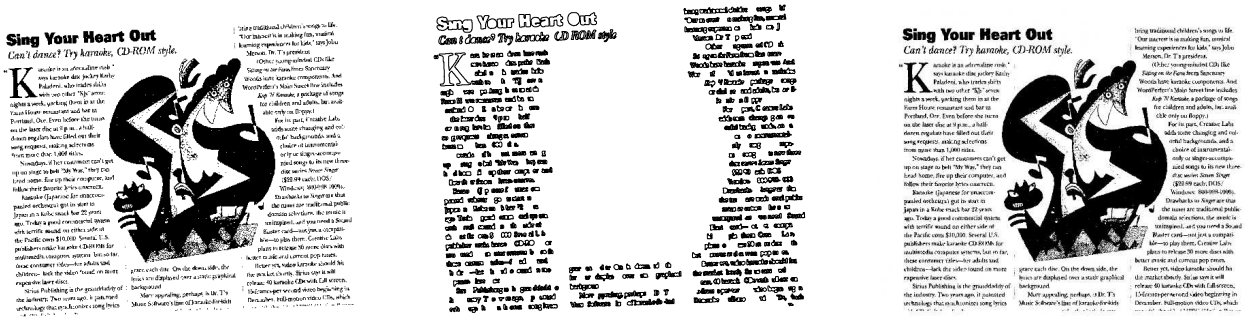

(a) (b) (c)

Figure 15: (a) Skewed page – image size 1100×900; (b) extracted region boundaries; (c) skew correction using $\mathcal{R}_S$ over scale.

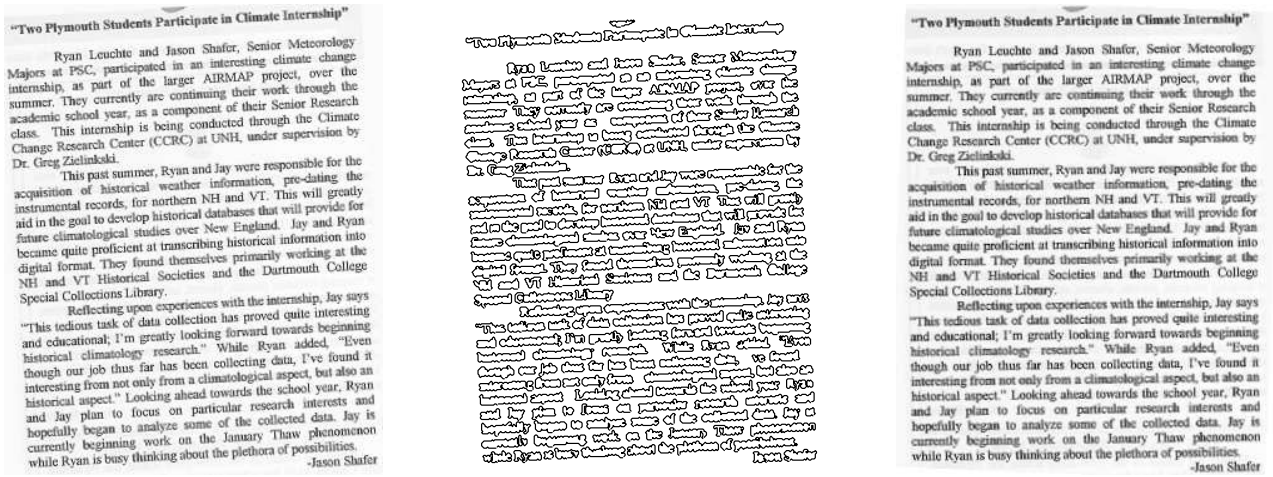

(a) (b) (c)

Figure 16: (a) Skewed page – image size 300×380; (b) extracted region boundaries; (c) skew correction using $\mathcal{R}_A$ over scale.

the contours individually deprojected are shown in figure 18c. Results are presented for $\mathcal{Q}_1$, but similar results were obtained using the other rectilinearity measures. The rectilinearity measure can be as easily applied to disjoint edges as single polygons, and figure 18d gives the result of deskewing all the contours as a single data set. The effect is similar except for the second top building which has been more accurately deskewed.

Finally, if a region is assumed to have an underlying rectilinear shape, obscured by noise and extraneous detail, then rectilinearity can be used to drive shape simplification which has particular application in cartography [16, 26]. In a similar approach to the extraction of natural scales of curves [22] a small discrete set of levels of simplification are automatically determined from the data. Rather than perform blurring of the curve as in [22] Ramer's polygonal approximation is used with a set of threshold values starting from one and increasing until the resultant polygon has only three lines. This generates a graph of rectilinearity versus threshold which we smooth slightly before locating peaks. As illustrated in figure 19 these correspond to shapes with qualitative differences in their appearance.

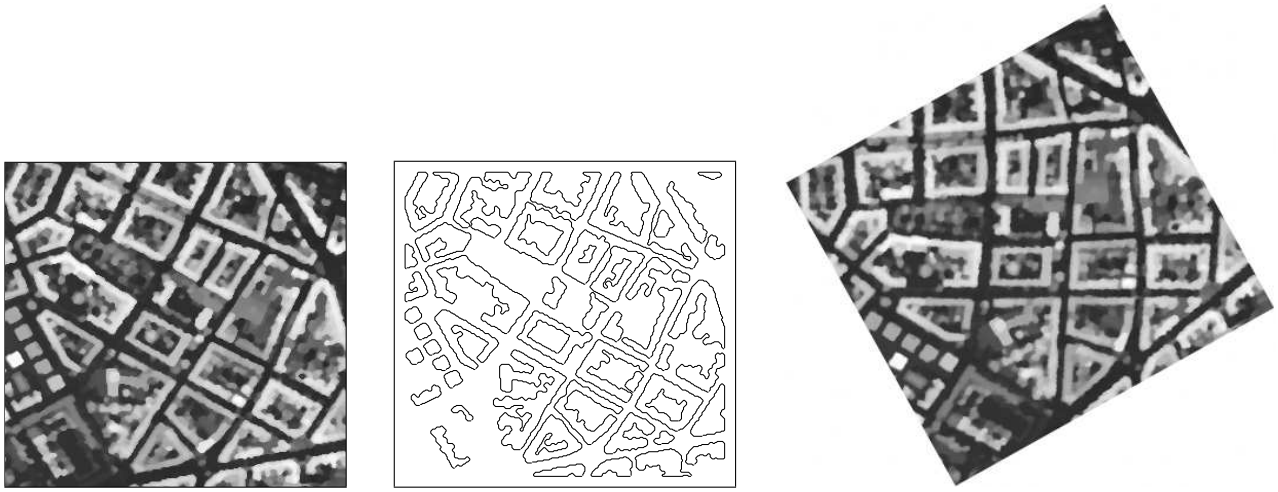

(a) (b) (c)

Figure 17: (a) A DEM of Hanover; (b) extracted region boundaries; (c) rotation maximising $\mathcal{Q}_1$ over scale.

5 Conclusions

Two new methods for computing the rectilinearity of shapes have been presented. In addition, an approach has been given for setting the algorithms in a scale-based context to overcome difficulties with spurious detail arising from quantisation errors, noise, etc. Testing on both synthetic and real data showed that in most cases the algorithms performed reliably and in accordance with human perception. Although operating on different principals (perimeter lengths versus angles) all the measures appeared to have similar performance. Previously several applications of rectilinearity measures were given [25]. Here we demonstrate further ones, namely skew correction of scanned documents, deprojection of aerial photographs of buildings, and scale selection for curve simplification, all of which emphasise the usefulness of the concept of a rectilinearity measure.

References

[1] P.G. Batchelor, A.D. Castellano Smith, D.L.G. Hill, D.J. Hawkes, T.C.S. Cox, and A.F. Dean. Measures of folding applied to the development of the human fetal brain. *IEEE Trans. on Medical Imaging*, 21(8):953–965, 2002.

[2] M. Beyer, R. Hahn, S. Peschel, M. Harz, and M. Knoche. Analysing fruit shape in sweet cherry (Prunus avium L.). *Scientia Horticulturae*, 96:139–150, 2002.

[3] J. Bogaert, R. Rousseau, P. Van Hecke, and I. Impens. Alternative area-perimeter ratios for measurement of 2D-shape compactness of habitats. *Applied Mathematics and Computation*, 111:71–85, 2000.

[4] F.L. Bookstein, A.P. Streissguth, P.D. Sampson, P.D. Connor, and H.M. Barr. Corpus callosum shape and neuropsychological deficits in adult males with heavy fetal alcohol exposure. *NeuroImage*, 15:233–251, 2002.

[5] E. Bribiesca. Measuring 2-d shape compactness using the contact perimeter. *CompMathApp*, 33(11), 1997.

[6] C. Di Ruberto and A. Dempster. Circularity measures based on mathematical morphology. *Electronics Letters*, 36(20):1691–1693, 2000.

[7] G.S. Dulikravich. Aerodynamic shape design and optimization: Status and trends. *Journal of Aircraft*, 29(6):1020–1026, 1992.

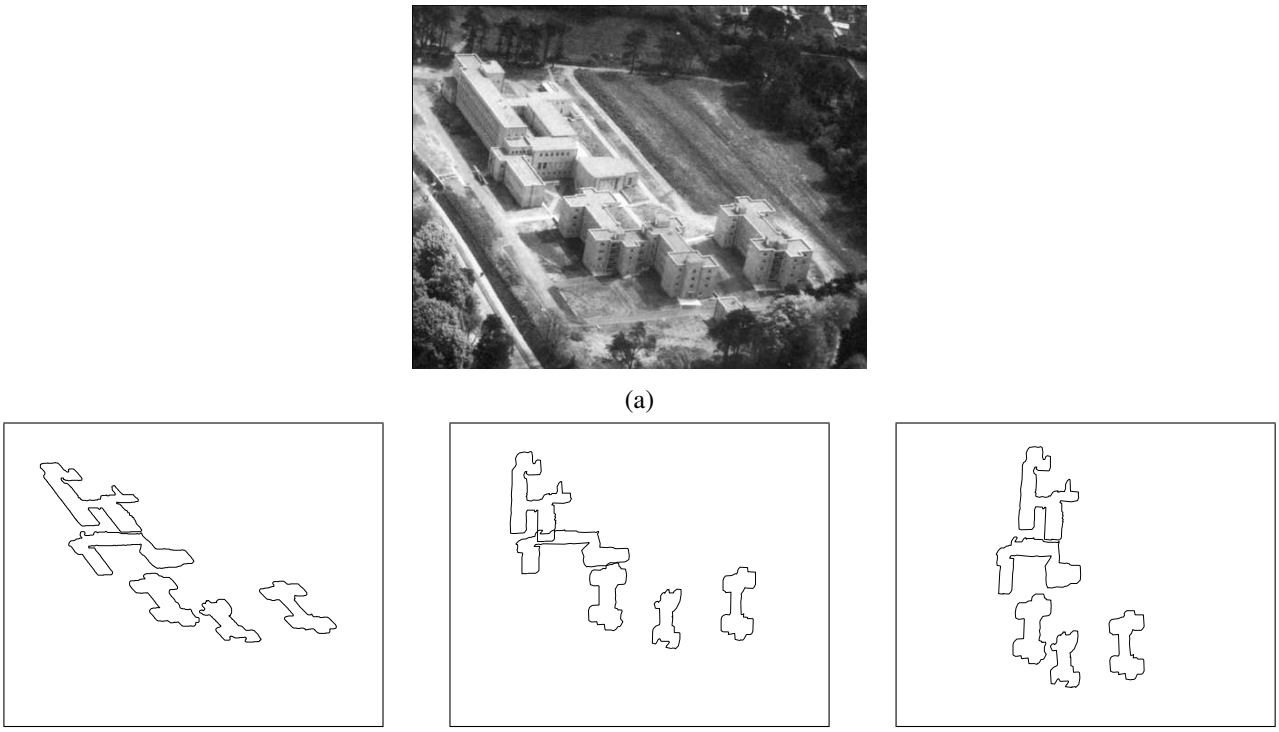

(a) (b) (c) (d)

Figure 18: (a) Aerial photograph of Cardiff, (b) extracted contours of buildings, (c) contours individually deskewed, (d) contour set globally deskewed.

[8] R. Gray and D. Regan. Accuracy of reproducing angles: is a right angle special? *Perception*, 25:531–542, 1996.

[9] M.A. Grayson. The heat equation shrinks embedded plane curves to round points. *Journal of Differential Geometry*, 26:285–314, 1987.

[10] R.M. Haralick. A measure for circularity of digital figures. *IEEE Trans. on Systems, Man and Cybernetics*, 4:394–396, 1974.

[11] K.P. Hinshaw, A.V. Poliakov, E.B. Moore, R.F. Martin, L.G. Shapiro, and J.F. Brinkley. Shape-based cortical surface segmentation for visualization brain mapping. *Medical Image Analysis*, 16:295–316, 2002.

[12] S.H.Y. Hung. On the straightness of digital arcs. *IEEE Trans. on Pattern Analysis and Machine Intelligence*, 7(2):203–215, 1985.

[13] D.W. Jacobs. Robust and efficient detection of salient convex groups. *IEEE Trans. on Pattern Analysis and Machine Intelligence*, 18(1):23–37, 1996.

[14] S. Loncaric. A survey of shape analysis techniques. *Pattern Recognition*, 31(8):983–1001, 1998.

[15] K.V. Mardia and P.E. Jupp. *Directional Statistics*. John Wiley, 1999.

[16] R.B. McMaster. Automated line generalization. *Cartographica*, 24(2):74–111, 1987.

[17] N.C. Mitchell. The transition from circular to stellate forms of submarine volcanoes. *J. Geophys. Res.*, 106:1987–2003, 2001.

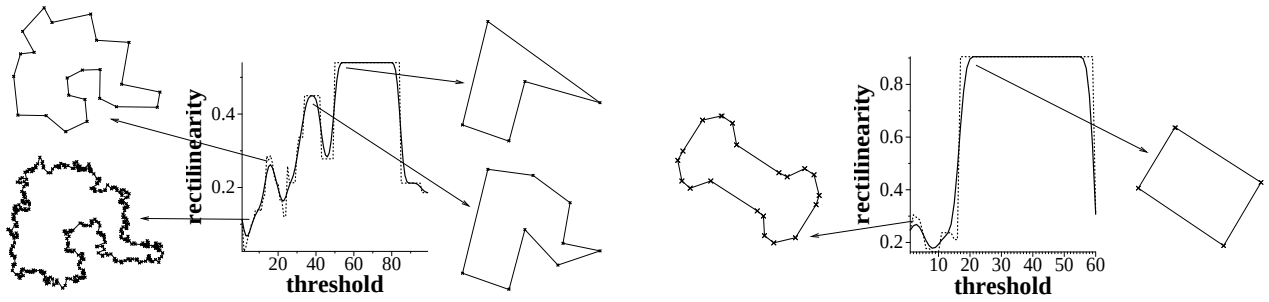

Figure 19: Graphs generated by forming polygonal approximations with different error thresholds. Peaks correspond to "natural scales" displaying qualitative changes in shape.

[18] H. Pao, D. Geiger, and N. Rubin. Measuring convexity for figure/ground separation. In *Int. Conf. Computer Vision*, pages 948–955, 1999.

[19] T. Pavlidis. A review of algorithms for shape analysis. *Computer Graphics and Image Processing*, 7(2):243–258, 1978.

[20] D. Proffitt. The measurement of circularity and ellipticity on a digital grid. *Pattern Recognition*, 15(5):383–387, 1982.

[21] U. Ramer. An iterative procedure for the polygonal approximation of plane curves. *Computer Graphics and Image Processing*, 1:244–256, 1972.

[22] P.L. Rosin. Representing curves at their natural scales. *Pattern Recognition*, 25:1315–1325, 1992.

[23] P.L. Rosin. Shape partitioning by convexity. *IEEE Trans. on Systems, Man and Cybernetics*, part A, 30(2):202–210, 2000.

[24] M.J. Rost, S.B. van Albada, and J.W.M. Frenken. Shape and decay of two- and three-dimensional islands on Au(1 1 0). *Surface Science*, 515:344–358, 2002.

[25] J. Žunić and P.L. Rosin. Rectilinearity measurements for polygons. *IEEE Trans. on Pattern Analysis and Machine Intelligence*, 25(9):1193–1200, 2003.

[26] Z. Wang and D. Lee. Building simplification based on pattern recognition and shape analysis. In *Proc. Spatial Data Handling Symposium*, 2000.